# Formation of single crystal sulfur supersaturated silicon based junctions by pulsed laser melting

Malek Tabbal,[a] Taegon Kim, Jeffrey M. Warrender,[b] and Michael J. Aziz
*Harvard School of Engineering and Applied Sciences, Cambridge, Massachusetts 02138*

B. L. Cardozo and R. S. Goldman
*Department of Materials Science and Engineering, University of Michigan, Ann Arbor, Michigan 48109-2136*

(Received 26 June 2007; accepted 18 September 2007; published 18 October 2007)

The authors demonstrate the formation of *pn* and $nn^+$ junctions based on silicon supersaturated with sulfur (up to 0.46 at. %) using a combination of ion implantation and pulsed laser melting. Silicon wafers were implanted at 200 keV $^{32}S^+$ to doses ranging from $1\times10^{15}$ to $1\times10^{16}$ ions/cm$^2$ and subsequently melted and resolidified by using a homogenized excimer laser pulse. Above a threshold laser fluence of $\sim$1.4 J/cm$^2$, the process produces a single crystal supersaturated alloy, free of extended defects, with a sharp junction between the laser melted layer and the underlying substrate, located near the maximum penetration of the melt front. Hall effect measurements indicate that the laser melted layers are *n* doped with a free carrier density up to $8\times10^{18}$/cm$^3$ that decreases by one-third upon postirradiation furnace annealing at 550 °C. Dark current-voltage measurements performed on these structures show good rectifying behavior. The photovoltaic characteristics of the junctions were enhanced by postirradiation annealing at 550–800 °C. These effects are attributed to the evolution of a population of point defects that survive the laser treatment. The influence of ion implantation dose, laser fluence, and annealing temperature on the properties of the junctions is also presented and discussed.  [DOI: 10.1116/1.2796184]

## I. INTRODUCTION

Recently, there has been significant interest in the optical and electronic properties of laser-microstructured chalcogen-laden silicon, a form of Si that shows enhanced optical absorption at wavelengths above and below the band gap.[1,2] For example, laser-microstructured chalcogen-laden silicon was recently used for the fabrication of Si-based electronic and optoelectronic devices including IR photodiodes,[3] photodetectors,[4] and electron emitters.[5] Typically, the material is synthesized by repeated femtosecond or nanosecond laser irradiation of Si wafers in $SF_6$, leading to sulfur-laden disordered silicon layers with about 10 $\mu$m tall spikes.[1,6,7] We recently demonstrated significant enhancement of the subband gap absorption,[8] with little surface damage or roughening, via the irradiation of sulfur-implanted silicon with a few spatially uniform nanosecond excimer laser pulses. Because excimer lasers are widely utilized for industrial processes, and smooth surfaces are well suited to many device architectures, this approach is very promising for a wide range of novel applications. However, to date, little is known about the structure and electronic properties of laser-microstructured chalcogen-laden silicon. In this article, we investigate the structural and electrical properties of excimer laser-crystallized Si ion implanted with sulfur at levels of several orders of magnitude above the solid solubility limit. The article focuses on the evaluation of the crystalline quality of the laser melted layers using channeling Rutherford backscattering spectrometry (C-RBS) and transmission electron microscopy (TEM), and on their electrical properties assessed using Hall effect and current-voltage (*I-V*) characterization performed in the dark and under simulated solar irradiation. The effect of implantation dose, laser fluence, and postirradiation thermal annealing on the properties of the junctions is also presented and discussed.

## II. EXPERIMENT

300 $\mu$m thick, single-side polished *n*-Si(111) (*P* doped, 1.2 k$\Omega$ cm, and $\sim10^{12}$ cm$^{-3}$), *n*-Si(001) (*P* doped and $\sim$5 $\Omega$ cm), and *p*-Si(001) (*B* doped, 5 $\Omega$ cm, and $\sim10^{15}$ cm$^{-3}$) were ion implanted at room temperature with 200 keV $^{32}S^+$ to doses ranging from $1\times10^{15}$ to $1\times10^{16}$ ions/cm$^2$. The ion implanted samples were then irradiated in ambient, using a spatially homogenized pulsed $XeCl^+$ excimer laser beam (308 nm, 25 ns full width at half maximum, and 50 ns total duration) with fluences of 1.0, 1.4, and 1.8 J/cm$^2$. In order to process a sufficiently large area ($1.5\times1.5$ cm$^2$), the samples were mounted on an *X-Y* stage and the $\sim3\times3$ mm$^2$ excimer laser spot was tiled across the area; consequently, the average point on the surface was irradiated by four to five pulses. Time-resolved reflectivity (TRR) of a low-power $Ar^+$ ion laser (488 nm) confirmed an optically flat surface and allowed us to monitor the duration over which the surface was molten. The $Ar^+$ ion laser beam

[a]On research leave from the Department of Physics, American University of Beirut, Beirut 1107 2020, Lebanon; electronic mail: malek.tabbal@aub.edu.lb
[b]Present address: Fatigue and Fracture Analysis Branch, Benet Laboratories, Watervliet, NY 12189.

is incident near the grazing angle on the Si surface and its reflected beam is detected by a fast photodiode that is connected to a digital oscilloscope in order to record the temporal variation of the reflected intensity. TRR was also used to calibrate the laser fluence by measuring the melt duration for a virgin crystalline Si wafer and to compare predictions of the melt depth versus fluence by a numerical solution of the one-dimensional heat equation using the well-established optical and thermophysical properties of crystalline, amorphous, and liquid silicon.[9,10] After the laser melting experiments, some samples were furnace annealed in flowing 99.999% Ar gas or in forming gas (10% $H_2$ and 90% $N_2$) for 30 min at temperatures ranging from 400 to 1000 °C.

The crystalline quality of the laser melted layers was quantified by Rutherford backscattering spectrometry in channeling mode (C-RBS) performed using 2 MeV $He^+$ ions down the [111] and [001] axes for the *n*-Si(111) and *p*-Si(001) substrates, respectively. Cross-sectional TEM (XTEM) examination was also carried out at 200 kV using a JEOL 2010F electron microscope, with lattice imaging obtained along the Si [110] direction. The surface morphology and roughness were investigated by *ex situ* atomic force microscopy using a MultiMode™ scanning probe microscope (NanoScope III) from Digital Instruments in tapping mode. The S concentration-depth profile in the laser melted layers were determined by secondary ion mass spectrometry (SIMS), as described elsewhere.[8] The carrier concentrations and carrier mobilities of the laser melted layers were determined using room-temperature resistivity and Hall measurements, both in the van der Pauw configuration.[11] In all cases, samples were cleaved into $0.6\times0.6$ $cm^2$ squares, and 99.99% indium solder contacts were applied. To determine the free carrier concentration $n_e$, the sheet carrier density (electrons/$cm^2$) is divided by the thickness of the S-incorporated layer determined from SIMS. To facilitate *I-V* measurements, electron beam evaporation was used to deposit, through a mask, narrow Cr–Au strips and metallic contact pads on top of the melted layers and on the back surface of the wafers, respectively. Current-voltage (*I-V*) measurements on the $nn^+$ and *pn* junctions were performed, at room temperature, in the dark and under an AM 1.5 solar simulator,[12] with 100 mW/$cm^2$ power density.

## III. RESULTS AND DISCUSSION

### A. Microstructural characterization

In Fig. 1, we present C-RBS spectra of S-implanted ($1\times10^{16}$ ions/$cm^2$) Si (111) substrates that were laser melted at different laser fluences. We also present the random and channeling spectra of the unimplanted virgin substrate and the channeling spectrum for the as-implanted wafers. In the latter spectrum, two distinct dechanneling peaks are observed, the first (~1130 keV) corresponds to the surface silicon atoms and the larger second peak (~1035 keV) arises from a heavily damaged crystalline or partly amorphous layer (~100 nm thick) buried beneath a more lightly damaged crystalline surface layer. The absence of a fully amorphous topmost damaged layer is indicative of surface heating by the incident ion beam during implantation. The peak of the damage is found to be at 210 nm, very close to the peak of the sulfur implant profile, which is located at 230 nm from the top surface, as measured by SIMS.[8] From the channeling spectra of the laser irradiated samples, it is clear that the crystallinity of the laser melted ion implanted layers is very sensitive to laser fluence. The strong dechanneling peak attributed to the buried amorphous/defective layer disappears for the sample irradiated at a laser fluence of 1.4 J/$cm^2$, as the C-RBS spectrum reveals a near-surface minimum backscattered yield $\chi_{min}$ —the ratio of the aligned to random yields—of about 4%, which is quite close to the value of 2.5% determined for the virgin single crystal Si substrate. Beyond a fluence threshold, pulsed laser melting of ion implanted silicon is known to melt the material to a depth greater than the defective region; the material then solidifies rapidly into highly supersaturated single crystalline material free of extended defects.[9,10] The channeling RBS spectrum from a sample irradiated at 1.8 J/$cm^2$ is nearly indistinguishable from the spectrum for a sample irradiated at 1.4 J/$cm^2$. These results were reproduced for *p*-Si(001) substrates and for different ion implantation doses. In addition, it was found that the $\chi_{min}$ measured from the C-RBS spectra of the laser melted samples (at 1.4 J/$cm^2$ and above) could be reduced to that of the virgin Si substrate upon annealing at 550 °C, which we attribute to point defect elimination by postirradiation anneals.

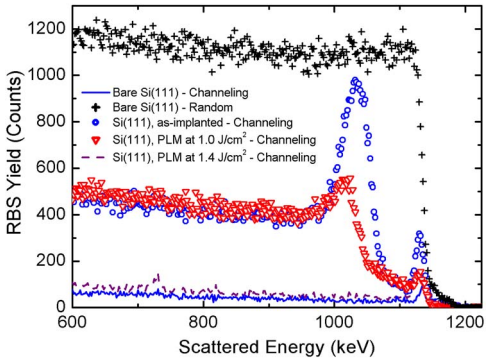


FIG. 1. Channeling RBS spectra of the following Si (111) substrates: unimplanted virgin (—), as implanted (○), implanted and pulsed laser melted (PLM) at 1.0 J/$cm^2$ (▽), and implanted and PLM at 1.4 J/$cm^2$ (---). The random spectrum of the virgin Si (111) wafer is also shown (+). The ion dose for the implanted spectra is $1\times10^{16}$ ions/$cm^2$. The peak at ~730 keV is from surface oxygen.

The high crystalline quality of the samples was further confirmed by XTEM, as shown in Fig. 2. No extended defects are observed and the transition between the implanted/laser melted layers and the underlying crystal is not distinguishable. In addition, atomic force microscopy (AFM) measurements indicate the occurrence of very little roughening of the surface of the wafers after laser melting. The surface roughness in $2\times2$ $\mu m^2$ AFM topographs was found to slightly increase from 0.21 nm, for layers implanted to a dose of $1\times10^{16}$ ions/$cm^2$, to 0.36 nm, following laser melting with 1.8 J/$cm^2$.

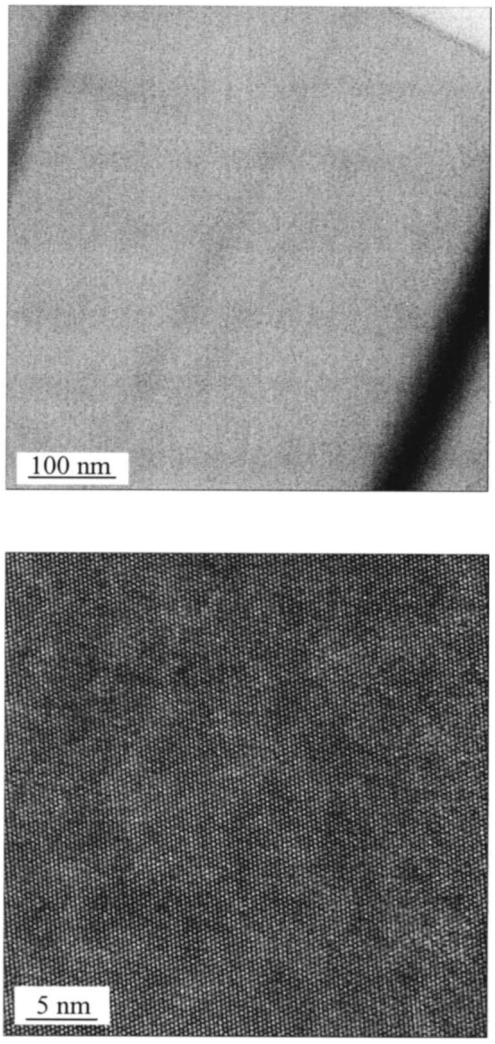


FIG. 2. (a) XTEM image of $n$-Si(111) sample implanted to a dose of $1\times10^{16}$ ions/cm$^2$ and irradiated at 1.8 J/cm$^2$, sample surface is in upper right. (b) Lattice resolution XTEM image of the same sample.

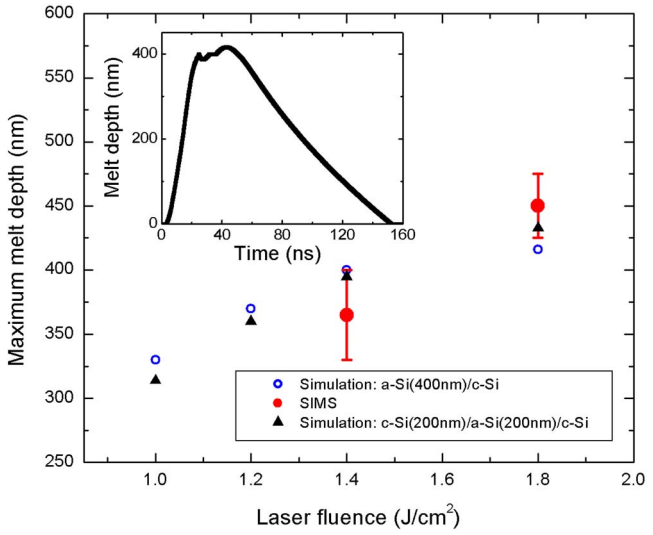


FIG. 3. Plot of the calculated maximum melt depth vs laser fluence for a structure consisting of a 200 nm thick $a$-Si layer buried at a depth of 200 nm in crystalline silicon (▲) and another consisting of 400 nm thick $a$-Si on top of the crystalline silicon substrate (○). Values inferred from SIMS (●) measurements are also shown with error bars.

Because estimating the melt depth induced by the laser is important for process control, heat flow simulations of melting and solidification were performed so the melt depth could be deduced from melt duration measurements. The calculated value of the maximum melt depth versus laser fluence is plotted in Fig. 3 for a structure consisting of a 200 nm thick amorphous Si ($a$-Si) layer buried under 200 nm of crystalline silicon and another consisting of a 400 nm thick $a$-Si layer on top of the crystalline silicon substrate. An example of the melt depth versus time from a simulation at a laser fluence of 1.8 J/cm$^2$ on a 400 nm $a$-Si layer is presented in the inset. The simulated melt depth versus fluence is consistent with the maximum melt depth inferred from the SIMS measurements. The SIMS concentration-depth profiles[8] indicated an abrupt drop in sulfur concentration at the maximum melt depth. The SIMS profiles also indicated no loss of sulfur upon laser melting. The results are qualitatively consistent with rapid solidification-induced solute trapping scenarios that are well documented for single laser shots on silicon implanted with other dopants.[13,14] In the case of sulfur documented here, it appears that we obtain supersaturated sulfur concentrations, as listed in Table I, exceeding by four orders of magnitude the equilibrium solubility limit.[15]

## B. Electrical characterization

The electrical properties of the samples are summarized in Table I. For all the laser melted S-implanted layers, the sign of the Hall coefficient indicates $n$-type conductivity. It is evident that $n_e$ increases with S implantation dose, reaching a

TABLE I. Total sulfur concentration, Hall mobility, free carrier concentration, and carrier-to-donor ratio in the laser melted layers for several implantation doses and a laser fluence of 1.8 J/cm$^2$.

| S dose (ions/cm$^2$) | S concentration (atoms/cm$^3$) | Hall mobility (cm$^2$/V s) | Carrier density ($e$/cm$^3$) | Carrier-to-donor ratio (%) |
|---|---|---|---|---|
| $1\times10^{15}$ | $2.3\times10^{19}$ | 200 | $7\times10^{17}$ | 3.0 |
| $3\times10^{15}$ | $7.7\times10^{19}$ | 69 | $3\times10^{18}$ | 3.9 |
| $1\times10^{16}$ | $2.3\times10^{20}$ | 61 | $8\times10^{18}$ | 3.5 |
| $1\times10^{16}$ +550 °C anneal | $2.3\times10^{20}$ | 184 | $5\times10^{18}$ | 2.1 |

maximum value of $8\times10^{18}$ electrons/cm$^3$ for a dose of $1\times10^{16}$ ions/cm$^2$. In contrast, the electron mobility decreases with S implantation dose, presumably due to increased ionized impurity scattering for higher doses.

For the unannealed laser melted samples, the ratio of free carrier density to total S concentration, which we termed as "carrier-to-donor" ratio, ranges from 3% to 4%. These low carrier-to-donor ratios may be due to the formation of S-induced midgap states in Si.[16]

SIMS measurements on laser melted samples subsequently annealed to temperatures as high as 900 °C reveal no change in retained S dose. In contrast to femtosecond laser microstructured Si:S, for which 40% of the sulfur could be lost upon annealing at a temperature of 450 °C,[6] there is no detectable loss and no detectable diffusion beyond the laser melt depth.[8] Therefore, the observed decrease in $n_e$ from $8\times10^{18}$ to $5\times10^{18}$ electrons/cm$^3$ for the annealed laser melted samples is due to a reduction in the carrier-to-donor ratio of the S dopants, rather than to a decrease in the total S incorporation in the layers. This drop in carrier-to-donor ratio upon annealing could be a consequence of the formation of precipitates or clusters with S or with native point defects at the expense of the total number of isolated S atoms in substitutional sites. The energetically favored form of isolated S atoms, substitutional sulfur,[17] forms electrically active dopants. Upon annealing, a clustering-induced decrease in electrically active substitutional S could occur. The formation of S clusters or precipitates could also explain the very limited diffusion of sulfur observed upon annealing to 900 °C. Their presence could not be confirmed by C-RBS or XTEM because of the very low S concentration in the layers,[8] namely, 0.46 at. %, for the highest implantation dose used in this work.

In contrast to the carrier-to-donor ratio, the mobility was significantly enhanced upon annealing, reaching 184 cm$^2$/V s for the sample implanted at $1\times10^{16}$/cm$^2$. This value is thrice that of the unannealed sample implanted at the same dose and is close to that of the unannealed sample implanted at the much lower dose of $1\times10^{15}$/cm$^2$. Because the ionized impurity concentration for the latter is nearly an order of magnitude less than that of the annealed sample, the annealing-induced electron mobility enhancement is not primarily due to a decrease in ionized impurity scattering. Post-laser melting annealing may lead to the removal or modification of other point defects, thereby reducing the scattering probability of the free carriers. For example, annealing may lead to the removal of vacancies known to be present in laser-crystallized implanted regions.[18,19] Additionally, annealing may enable the evolution of inactive point defects from a charged to a neutral configuration, thereby reducing the scattering probability of the free carriers.[20]

In Fig. 4, we present the dark current versus voltage ($I$-$V$) characteristics of the *pn* junctions formed by laser melting at 1.8 J/cm$^2$ of *p*-doped Si substrates implanted to a dose of $1\times10^{16}$ S/cm$^2$ and annealed at various temperatures up to 1000 °C. All curves show good rectifying behavior except for the one corresponding to the highest annealing temperature, which has poor forward current characteristics and a significantly high leakage current, $I_L$ (0.85 mA/cm$^2$ at −0.5 V). The lowest value of $I_L$ at −0.5 V was 0.064 mA/cm$^2$, obtained for the nonannealed layers. The ideality factor $n$ was determined by fitting the forward current $I_F$ to the relationship[21]

$$I_F \sim \exp(qV/nkT),$$

where $q$ is the charge of the electron, $kT$ is the thermal energy, and $V$ is the applied voltage. An ideality factor of 2.06 was determined for the junctions annealed at 550 °C, a value that is very close to the value of 2 which is an indication of bulk recombination of the charge carriers occurring in the depletion region.[21]

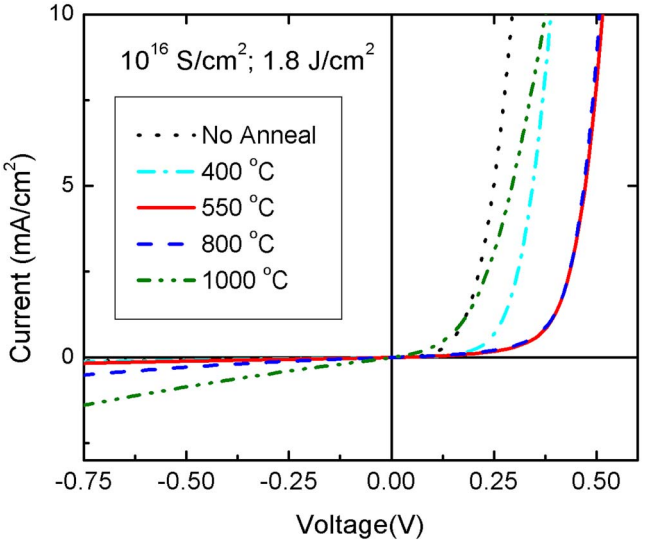


FIG. 4. Dark $I$-$V$ curves measured for *p*-Si(001) samples implanted at a dose $1\times10^{16}$/cm$^2$, irradiated at 1.8 J/cm$^2$, and furnace annealed at different temperatures.

In Fig. 5, we present the $I$-$V$ curves of the same *pn* junc-

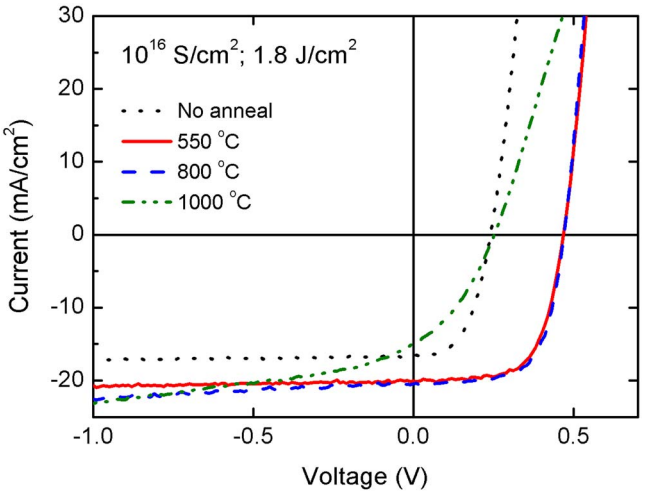


FIG. 5. $I$-$V$ curves measured under one sun for *p*-Si(001) samples implanted to a dose of $1\times10^{16}$/cm$^2$, irradiated at 1.8 J/cm$^2$, and furnace annealed at different temperatures.

tions measured under one sun (AM 1.5 and 100 mW/cm$^2$) for different annealing temperatures. In agreement with the dark current measurements reported in Fig. 4, annealing at 550 or 800 °C leads to an increased short circuit current, $I_{sc}$, and open circuit voltage, $V_{oc}$, but a further increase in annealing temperature to 1000 °C results in a significant reduction. With the 550 °C annealed samples, values of 20 mA/cm$^2$ and 470 mV were measured for the $I_{sc}$ and $V_{oc}$, respectively, leading to a fill factor >65% and an energy conversion efficiency >6%. It should be noted that these latter values were obtained without any solar cell device engineering such as the application of an antireflection coating on the top surface, the formation of a back-surface field, base doping, or top electrode geometry optimization. With device engineering, the short absorption length[2,8] of these structures might present an opportunity for advances in thin film silicon photovoltaics.

We attribute the increase in the values of $V_{oc}$ and $|I_{sc}|$ upon annealing at 550 °C to a decrease in the density of point defects, which was proposed as one of the two mechanisms that lead to the observed increase in mobility reported in Table I. Indeed, point defects that survive the laser melting process can act as recombination centers for photogenerated carriers; their subsequent annealing would improve the photovoltaic characteristics of the junctions. This does not exclude the presence of the other mechanism—namely, the neutralization of ionized dopants—as deduced from the measured drop in the value of $n_e$ from $8\times10^{18}$ to $5\times10^{18}$ electrons/cm$^3$ upon annealing (see Table I). However, the effect of this drop in $n_e$ on the value of $V_{oc}$ would be a decrease of a few percent, which is likely to be masked by the enhancement of $V_{oc}$ due to point defect annealing. Although the C-RBS spectra and the XTEM micrographs (Figs. 1 and 2, respectively) indicate that laser irradiation at 1.8 J/cm$^2$ results in the formation of a single crystal supersaturated with S and free of extended defects, the presence of point defects that are undetectable by C-RBS and XTEM cannot be ruled out. They could be located either within the melted layers during solidification or they could be generated by the ion implantation process in the channeled tail beneath the amorphous layer. In the latter case, this ion implantation damage region would extend beyond the laser melt depth (~450 nm at 1.8 J/cm$^2$) and, therefore, postirradiation annealing would be necessary to reduce the density of these defects. It is also noteworthy that the enhancement of the electrical characteristics of the junctions was found to be independent of the ambient gas flowing during the annealing process, as the use of Ar or forming gas led to similar *I-V* characteristics of the junctions. Therefore, any hydrogen passivation mechanism of point defects (such as dangling bonds) plays only a minor role in improving the electrical properties of the junctions. For anneals at the very high temperature of 1000 °C, excessive clustering or precipitation of the S dopants is expected to occur,[17] thereby degrading the electrical properties of the junctions. These two competing phenomena would explain the occurrence of a window of annealing temperatures for good rectifying and photovoltaic behaviors of the junctions.

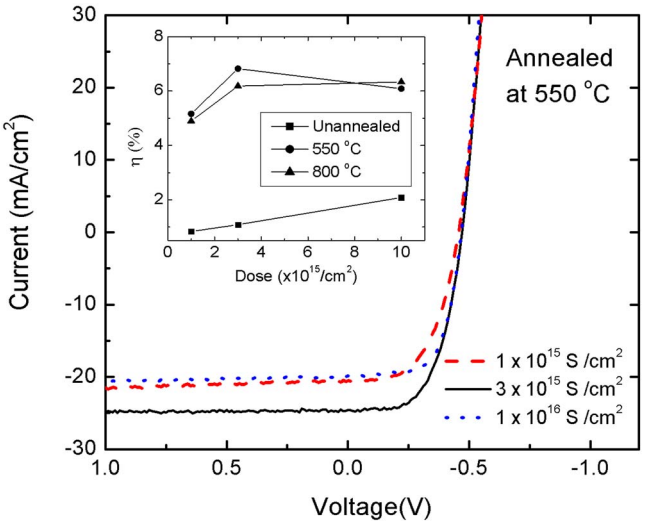


FIG. 6. *I-V* curves measured under one sun for samples implanted with different ion doses in *p*-Si(001), irradiated at 1.8 J/cm$^2$, and furnace annealed at 550 °C. The inset shows the variation of the efficiency $\eta$ vs ion implantation dose for different annealing temperatures.

The effect of annealing on the *I-V* characteristics of the samples implanted for various doses is presented in Fig. 6. The value of $V_{oc}$ is nearly independent of implantation dose at (470±10) mV. The value of $I_{sc}$ is significantly higher (~25 mA/cm$^2$) for the medium dose of $3\times10^{15}$ S/cm$^2$. However, the increase in photocurrent measured for the medium dose sample is accompanied by a loss in fill factor, resulting in almost no change in efficiency, as is seen in the inset. The trend is consistent with the effects of annealing shown in Figs. 4 and 5.

Finally, preliminary electrical characterizations were also carried out on laser melted S implanted *n*-Si(001) substrates. Because sulfur acts as a donor, $nn^+$ homojunctions were thus formed, with the $n^+$ region being the implanted/laser irradiated top layers. Dark *I-V* curves from two such homojunctions are presented in Fig. 7. Both curves show a good rectifying behavior with a built-in voltage $V_{bi}$ lower than those observed for the *pn* junction. This is justified by observing that, for a $nn^+$ junction, the $V_{bi}$ is given by the following expression:

$$V_{bi} = (kT/q)\ln(n^+/n),$$

where $n^+$ and $n$ are the free charge carrier concentrations in the highly doped region and underlying substrate, respectively. In our case, the ratio $n^+/n$ is of the order of 1000 (~$10^{18}/10^{15}$), thereby leading to a $V_{bi}$ of 0.17 eV. The junction annealed at 550 °C shows better *I-V* characteristics than the one annealed at 1000 °C, as inferred from a lower leakage current and a lower ideality factor in forward bias (~2.1 vs 3, respectively). These observations are consistent with the results presented above for the *pn* junctions, where an

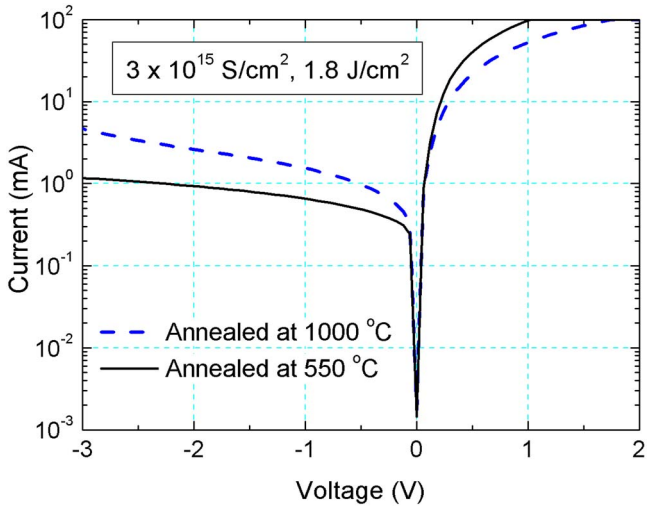


FIG. 7. Dark *I-V* curves corresponding to *n*-Si(001) substrates implanted to a dose of $3\times10^{15}/\mathrm{cm}^2$, laser irradiated at 1.8 $\mathrm{J/cm}^2$, and subsequently annealed at 550 or 1000 °C.

annealing temperature window appears to enhance the electrical characteristics of the junctions.

## IV. SUMMARY

We have investigated the crystalline and electrical properties of silicon with 0.46 at. % of sulfur in supersaturated solid solution. This novel material was synthesized by ion implantation of sulfur into Si wafers followed by pulsed laser melting–induced rapid solidification using an excimer laser. The low number of laser pulses used in this work ensures little irradiation-induced surface damage or roughening of the wafers. The crystalline quality of the layers after laser irradiation was evaluated by channeling RBS and TEM. It was shown that laser fluences of 1.4 $\mathrm{J/cm}^2$ and above are necessary to melt through the amorphous implanted region leaving, after solidification, a perfect single crystal free from extended defects. By performing experiments on *p*-doped and *n*-doped substrates, *pn* and $nn^+$ junctions were formed and showed good rectifying and photovoltaic behaviors. The properties of the junctions were enhanced by postirradiation furnace anneals, with samples annealed within a window of 550–800 °C exhibiting good properties. We attribute the improvement in properties upon annealing to the annihilation of point defects that survive the laser melting and rapid solidification process. We attribute the deterioration upon annealing at 1000 °C to clustering or precipitation of the sulfur atoms. The junctions could be further optimized by applying the appropriate device engineering processes. The short absorption length of these structures might present an opportunity for advances in thin film silicon photovoltaics, but there remain many unanswered questions regarding, e.g., band structure and minority carrier diffusion lengths.

Excimer laser melting combined with ion implantation is shown to be a controllable and well characterized technique that enables the production of unusual compositions in stable, supersaturated solid solution, making it potentially attractive for the fabrication of electronic and optoelectronic devices based on chalcogen-laden Si.

## ACKNOWLEDGMENTS

The authors thank E. Mazur, J. E. Carey, E. Kaxiras, Y. Mo, F. Capasso, and J. Bao for helpful discussions. This work was supported by National Science Foundation Grant No. DMR-0306997. One of the authors (M.T.) acknowledges the financial support of the Arab Fund and Fulbright programs and another author (R.S.G.) a Radcliffe Institute Fellowship. T.G.K. was supported by the Korea Research Foundation Grant funded by the Korean Government (MOEHRD, Basic Research Promotion Fund), Grant No. KRF-2004-214-C00156. B.L.C. and R.S.G. were supported by the U.S. Department of Defense through the Intelligence Community Postdoctoral Fellowship under Grant No. HM1582-05-1-2027. Central facilities were used within the Harvard Center for Nanoscale Systems.

[1] C. H. Crouch, J. E. Carey, J. M. Warrender, E. Mazur, M. J. Aziz, and F. Genin, Appl. Phys. Lett. **84**, 1850 (2004).
[2] C. Wu *et al.*, Appl. Phys. Lett. **78**, 1850 (2001).
[3] J. E. Carey, C. H. Crouch, M. A. Sheehy, M. Shen, C. M. Friend, and E. Mazur, Opt. Lett. **30**, 1773 (2005).
[4] Z. Huang, J. E. Carey, M. Liu, X. Guo, E. Mazur, and J. C. Campbell, Appl. Phys. Lett. **89**, 033506 (2006).
[5] V. Zorba, P. Tzanetakis, C. Fotakis, E. Spanakis, E. Stratakis, D. G. Papazoglou, and I. Zergioti, Appl. Phys. Lett. **88**, 081103 (2006).
[6] C. H. Crouch, J. E. Carey, M. Shen, E. Mazur, and F. Y. Genin, Appl. Phys. A: Mater. Sci. Process. **79**, 1635 (2004).
[7] A. J. Pedraza, J. D. Fowlkes, and D. H. Lowndes, Appl. Phys. Lett. **74**, 2322 (1999).
[8] T. G. Kim, J. M. Warrender, and M. J. Aziz, Appl. Phys. Lett. **88**, 241902 (2006).
[9] M. J. Aziz, C. W. White, J. Narayan, and B. Stritzker, in *Energy Beam-Solid Interactions and Transient Thermal Processing*, edited by V. T. Nguyen and A. G. Cullis (Editions de Physique, Paris, 1985), p. 231.
[10] R. Reitano, P. M. Smith, and M. J. Aziz, J. Appl. Phys. **76**, 1518 (1994).
[11] L. J. van der Pauw, Philips Res. Rep. **13**, 1 (1958).
[12] ThermalOriel model 66902 sun simulator.
[13] M. J. Aziz, Metall. Mater. Trans. A **27**, 671 (1996).
[14] J. A. Kittl, P. G. Sanders, M. J. Aziz, D. P. Brunco, and M. O. Thompson, Acta Mater. **48**, 4797 (2000).
[15] R. G. Wilson, J. Appl. Phys. **55**, 3490 (1984).
[16] E. Janzen, R. Stedman, G. Grossmann, and H. G. Grimmeiss, Phys. Rev. B **29**, 1907 (1984).
[17] Y. Mo, M. Z. Bazant, and E. Kaxiras, Phys. Rev. B **70**, 205210 (2004).
[18] G. Mannino, V. Privitera, A. La Magna, E. Rimini, E. Napolitani, G. Fortunato, and L. Mariucci, Appl. Phys. Lett. **86**, 051909 (2005).
[19] L. Romano, A. M. Piro, V. Privitera, E. Rimini, G. Fortunato, B. G. Svensson, M. Foad, and M. G. Grimaldi, Nucl. Instrum. Methods Phys. Res. B **253**, 50 (2006).
[20] Y. Takamura, S. H. Jain, P. B. Griffin, and J. D. Plummer, J. Appl. Phys. **92**, 230 (2002).
[21] S. M. Sze, *Physics of Semiconductor Devices* (Wiley, New York, 1981), p. 68.